Eberswalde University
for Sustainable
Development

Multi-Sensor Analysis of Land Surface Temperature and Sentinel-1 SAR Backscatter in Dresden, Summer 2023

Advanced Remote Sensing Innovations (ARSI)

Submitted to
Prof. Dr. Jan-Peter Mund
Chair of GIS and Remote Sensing
HNEE, Eberswalde

Submission date: 20 February 2026

Submitted by
Mahbubul Alam
Masters in Forest Information Technology
Matrikel Nr. 24215867

Abstract

Urban areas show strong spatial differences in surface temperature, mainly influenced by land cover, building density, and vegetation. This study combines Land Surface Temperature (LST) from Landsat 8/9 with Sentinel-1 C-band SAR backscatter to analyse the summer thermal and structural patterns of Dresden, Germany, for June–August 2023. All data processing — including filtering, cloud masking, compositing, and map generation — was carried out in Google Earth Engine (GEE). LST was retrieved from the Landsat Collection 2 Level-2 product using USGS scaling factors, while Sentinel-1 GRD data in IW mode were used to produce VV and VH backscatter composites and the VV–VH polarisation ratio. The statistical evaluation included scatter plots, a Pearson correlation matrix, box-plot comparisons, a histogram of LST values, and a multivariate pair plot. A weak to moderate positive correlation ($r = 0.28$) was found between VV backscatter and LST, reflecting the tendency of dense built-up areas to exhibit both higher structural roughness and elevated surface temperatures. Vegetated zones and water bodies consistently showed low backscatter and lower LST, while sealed surfaces formed the main thermal hotspots. The LST histogram displayed a clear bimodal pattern, mainly due to the contrast between the cool Dresdner Heide forest and the warmer urban fabric.A notable finding was that pixels classified as “built-up” using a simple VV threshold showed a lower median LST than the remaining pixels. This highlights the limitations of threshold-based SAR classification in heterogeneous landscapes, where bare agricultural fields can reach high temperatures. Overall, the study demonstrates the complementary value of combining thermal infrared and SAR data in GEE and emphasises the need for more advanced, supervised approaches for analysing urban heat patterns.

Keywords: *Land Surface Temperature, Synthetic Aperture Radar, Sentinel-1, Landsat 8/9, Urban Heat Island, Google Earth Engine, Dresden, VV–VH Ratio, Polarisation Ratio*

\

Acknowledgement

I would like to thank Prof. Dr. Jan-Peter Mund for his guidance, methodological support, and for providing the data and framework used in this project. I am also grateful for the helpful discussions and collaboration within the course, which contributed to a productive learning environment. This report was prepared with the assistance of digital writing tools. Grammarly was used to refine grammar and readability, while Microsoft Copilot supported the structuring of sections and the organisation of ideas. All interpretations, analyses, and conclusions presented in this report are entirely my own.

List of Abbreviations

Abbreviation	Full Term
AOI	Area of Interest
C-band	C-frequency band (~5.4 GHz, Sentinel-1 SAR)
DN	Digital Number (raw satellite sensor value)
dB	Decibel (logarithmic unit of backscatter intensity)
DEM	Digital Elevation Model
EMU	English Metric Units (used in OOXML image sizing)
ESA	European Space Agency
GEE	Google Earth Engine
GRD	Ground Range Detected (Sentinel-1 processing level)
IW	Interferometric Wide (Sentinel-1 acquisition mode)
LST	Land Surface Temperature
MODIS	Moderate Resolution Imaging Spectroradiometer
NCEP	National Centers for Environmental Prediction
NDVI	Normalised Difference Vegetation Index
OLI	Operational Land Imager (Landsat 8/9 sensor)
SAR	Synthetic Aperture Radar

SRTM	Shuttle Radar Topography Mission
SUHI	Surface Urban Heat Island
TIR / TIRS	Thermal Infrared (Sensor) — Landsat Band 10
UHI	Urban Heat Island
USGS	United States Geological Survey
UTM	Universal Transverse Mercator (coordinate projection)
VH	Vertical transmit / Horizontal receive (SAR polarisation)
VV	Vertical transmit / Vertical receive (SAR polarisation)
σ^0	Sigma-nought (radar backscatter cross-section, dB)

Contents

List of Figures

1. Introduction

1.1 Background

Urbanisation fundamentally alters the thermal, hydrological, and radiative behaviour of the land surface. As natural and agricultural areas are replaced by impervious materials such as asphalt, concrete, and metal, cities tend to accumulate and retain heat, leading to the well-known Urban Heat Island (UHI) effect (Oke, 1982; Voogt & Oke, 2003). Satellite remote sensing has become an essential tool for analysing these thermal patterns. Landsat's thermal infrared sensors enable the retrieval of Land Surface Temperature (LST) at medium spatial resolution, making them widely used in UHI research. At the same time, Synthetic Aperture Radar (SAR) provides structural information related to surface roughness, geometry, and dielectric properties, independent of cloud cover and illumination.

Sentinel-1 SAR, with its dual VV and VH polarisation channels, captures scattering behaviour that reflects differences between built-up and vegetated surfaces. Combining thermal and SAR observations therefore offers a more complete understanding of how urban surfaces behave both thermally and structurally. Dresden, with its mixture of dense historical districts, suburban housing, industrial zones, the Elbe floodplain, and the extensive Dresdner Heide forest, provide an ideal setting for such a multi-sensor analysis.

1.2. Problem Statement

Thermal remote sensing alone cannot fully explain spatial variations in urban surface temperature because it does not capture structural characteristics such as building geometry, surface roughness, or moisture-related dielectric properties. Conversely, SAR backscatter provides valuable structural information but does not measure temperature. Although these two sensor types are highly complementary, integrated thermal–SAR studies remain limited for medium-sized Central European cities. As a result, our understanding of how built-up and vegetated areas differ in both thermal behaviour and radar scattering remains incomplete.

1.3. Research Question

To address this gap, the study is guided by the following research question:

How do built-up and non-built-up areas in Dresden differ in their Land Surface Temperature and Sentinel-1 VV/VH backscatter characteristics during the summer of 2023?

This question provides a clear analytical focus and links directly to the project's objectives.

1.4 Objectives

The study pursues the following objectives:

1. To retrieve and map Land Surface Temperature (LST) using Landsat 8/9 Collection 2 Level-2 thermal products.
2. To process Sentinel-1 GRD imagery in order to generate VV, VH, and VV–VH polarisation ratio layers.
3. To compare thermal and radar surface characteristics between built-up and non-built-up areas within the Dresden administrative boundary.
4. To quantify statistical relationships between LST and Sentinel-1 backscatter variables through correlation analysis and pixel-wise comparisons.
5. To develop an integrated multi-sensor interpretation of Dresden's urban surface conditions during summer 2023.

2. Literature Review

2.1 Urban Heat Island and Land Surface Temperature

The Urban Heat Island (UHI) effect has been recognised since Howard's early observations in 1833, showing that cities tend to be warmer than their rural surroundings. Later work by Oke (1982) explained this pattern through changes in the urban energy balance, including reduced sky-view factor, lower evapotranspiration, and the thermal properties of built materials. With the development of satellite thermal infrared sensors, research shifted toward analysing the surface UHI (SUHI), which can be directly observed from space (Voogt & Oke, 2003).

Landsat has played a central role in SUHI studies. Single-channel LST retrieval methods applied to Landsat Band 10 have been shown to produce reliable temperature estimates, typically within 1–2 K of ground measurements (Weng, 2009; Li et al., 2013). The Landsat 8/9 TIRS instruments further improved radiometric performance, with Band 10 recommended for operational LST retrieval due to stray-light issues in Band 11 (Barsi et al., 2014). The USGS Collection 2 Level-2 product used in this study incorporates these corrections and provides atmospherically adjusted LST (USGS, 2023).

Urban LST patterns are strongly linked to land cover. Vegetation consistently lowers surface temperature, as demonstrated by negative LST–NDVI relationships (Yuan & Bauer, 2007). Impervious surfaces, by contrast, can be 5–10°C warmer than vegetated areas (Stathopoulou & Cartalis, 2007). Broader studies across Europe show that SUHI intensity varies with urban form and green-space distribution, and can intensify during heat waves (Zhou et al., 2014; Gabriel & Endlicher, 2011). Dresden's mix of dense urban areas, forest, and river floodplain makes it representative of many medium-sized Central European cities.

2.2 Sentinel-1 SAR Backscatter in Urban Environments

SAR backscatter in cities is shaped by the interaction of microwave signals with buildings and other structured surfaces. At C-band, the dominant mechanism in dense urban areas is double-bounce scattering between vertical facades and horizontal surfaces, producing strong VV backscatter (Ulaby et al., 1982; Brunner et al., 2010). Sentinel-1's Interferometric Wide (IW) mode provides consistent dual-polarisation (VV/VH) coverage at 10 m resolution, making it widely used for urban mapping (Torres et al., 2012).

VH backscatter responds more strongly to vegetation due to volumetric scattering within canopies (Cloude & Pottier, 1996). The VV–VH ratio therefore enhances the contrast between built-up and vegetated areas and is frequently used for urban extent mapping (Antropov et al., 2014; Esch et al., 2017). Seasonal median compositing, as applied in this study, helps reduce noise from rainfall-related moisture variations and other short-term effects.

2.3 Integrating Thermal and SAR Data

Combining thermal infrared and SAR data has become increasingly feasible with cloud-based platforms such as Google Earth Engine (Gorelick et al., 2017). Several studies have reported positive correlations between VV backscatter and LST, reflecting the co-location of dense built-up areas with both high structural roughness and elevated temperatures (Zhang et al., 2016). SAR variables have also been used in machine-learning models to distinguish impervious from non-impervious surfaces, further linking radar scattering behaviour to thermal patterns (Dong et al., 2019).

However, the LST–SAR relationship is influenced by several confounding factors. Mixed pixels at 30 m resolution can combine vegetation, buildings, and bare soil. Moist surfaces increase SAR backscatter but often reduce LST due to evaporative cooling. Building orientation affects SAR but not thermal emission, and vegetation seasonality influences VH independently of temperature (Voogt & Oke, 2003; Brunner et al., 2010). These factors explain why correlations are typically moderate rather than strong.

This study contributes to the existing literature by analysing these relationships specifically for Dresden, a morphologically diverse Central European city that has not yet been examined using a combined Landsat–Sentinel-1 approach within a cloud-based processing environment.

3. Study Area

The study area is the administrative municipality of Dresden (Landeshauptstadt Dresden) in the federal state of Saxony, eastern Germany, centred at approximately 51.05°N and 13.74°E. With a population of around 560,000 residents in 2023 and a total area of roughly 328 km² (Statistical Office of Saxony, 2023), Dresden represents one of Germany's larger medium-sized cities. The River Elbe flows east–west through the urban core before turning northward, forming a major hydrological corridor that influences local microclimates and surface temperatures (Gabriel & Endlicher, 2011).

Dresden's land cover is highly heterogeneous. The compact historical centre (Innere Altstadt) contains dense multi-storey buildings, while post-war prefabricated housing estates (Plattenbaugebiete) dominate parts of the northern and eastern districts. Suburban neighbourhoods consist mainly of single- and two-family homes with gardens and street trees.

Industrial and logistics zones are concentrated along the western and southern periphery. The Elbe floodplain meadows (Elbwiesen) form a continuous band of riparian grassland and scattered woodland, while the Dresdner Heide — a managed forest of approximately 58 km² — represents the largest vegetated area within the municipal boundary (City of Dresden, 2023). Agricultural fields and small settlements occupy the outer periphery. This mosaic of built-up, vegetated, and open surfaces creates strong spatial contrasts in both LST and SAR backscatter, making Dresden an ideal test site for multi-sensor surface characterisation.

Climatically, Dresden lies in a temperate transition zone between oceanic and continental influences (Köppen Cfb/Dfb), with a mean annual temperature of about 10°C and a mean July temperature of roughly 19°C (DWD, 2023). The summer of 2023 included several heat-wave episodes across Germany, with maximum temperatures in Dresden exceeding 35°C on multiple days, providing representative conditions for analysing peak UHI intensity (DWD, 2023). All spatial analyses in Google Earth Engine were clipped to the official administrative boundary of Dresden (Dresden1.shp), retrieved from OpenStreetMap using the QuickOSM plugin in QGIS (OpenStreetMap Contributors, 2023). This ensured consistent spatial coverage across all datasets and avoided discrepancies between Landsat and Sentinel-1 footprints.

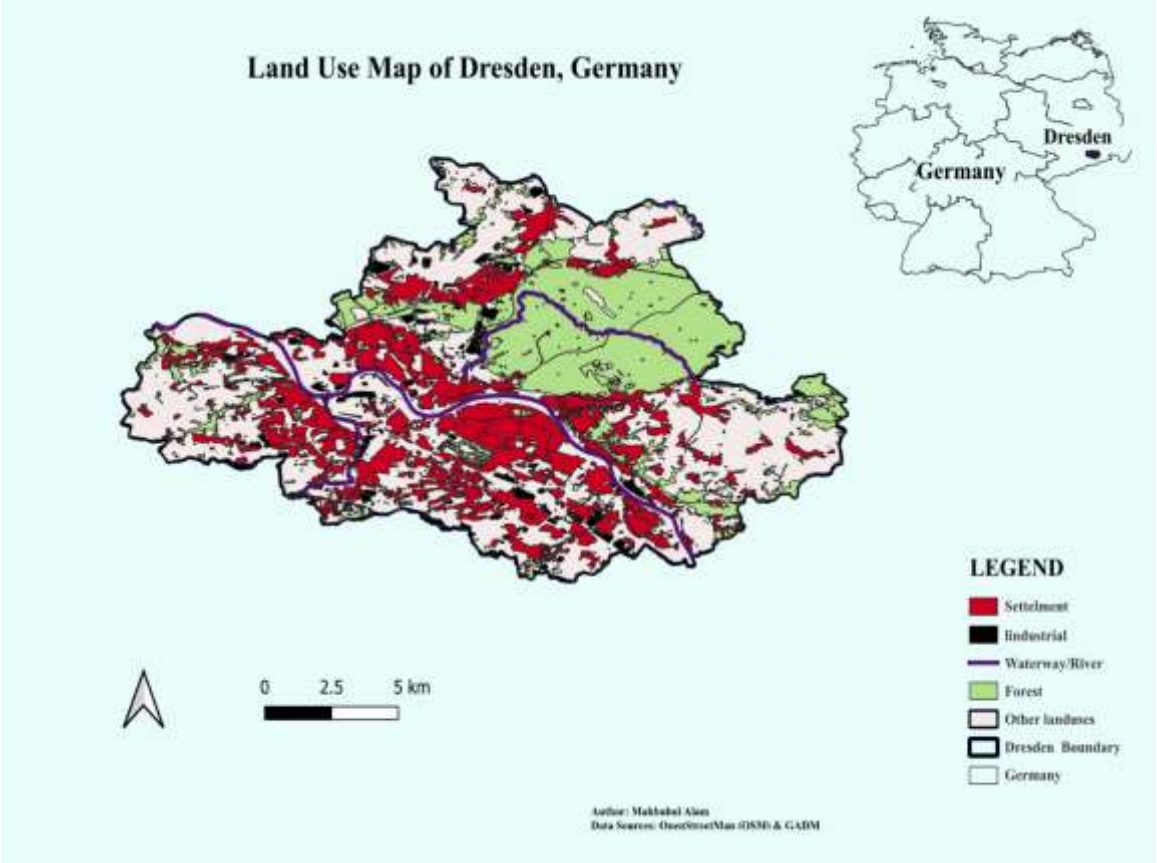

Figure 1: Study Area

4. Data and Methods

This study integrates multispectral thermal data from Landsat 8/9 with C-band SAR observations from Sentinel-1 to analyse spatial patterns of surface temperature and radar backscatter across Dresden. The analysis focuses on four variables: **LST** (Land Surface Temperature), **VV** (co-polarised backscatter), **VH** (cross-polarised backscatter), and **VV–VH** (polarisation ratio in dB). These variables together provide a compact representation of the thermal and structural properties of the urban surface. All preprocessing, compositing, and spatial analysis were performed in Google Earth Engine (GEE), while statistical evaluation and visualisation were completed in Python. The workflow consists of four main components: (i) GEE-based data preparation, (ii) Landsat-derived LST retrieval, (iii) Sentinel-1 SAR backscatter processing, and (iv) inter-sensor statistical comparison.

4.1 Google Earth Engine Processing Framework

All satellite data acquisition, preprocessing, compositing, and mapping were carried out in Google Earth Engine (Gorelick et al., 2017). GEE provides direct access to the full Landsat and Sentinel archives and enables large-scale pixel-wise operations without local downloads. The workflow implemented in the GEE JavaScript API included filtering by area of interest (AOI), date range, and sensor metadata; cloud masking; calculation of derived variables; median compositing; clipping to the Dresden administrative boundary; and exporting analysis-ready GeoTIFFs. Spatial visualisations were produced directly in the GEE code editor. Subsequent statistical analyses were performed in Python (v3.10) using NumPy, Pandas, Matplotlib, Seaborn, and Rasterio.

4.2 Landsat 8/9 Land Surface Temperature Retrieval

LST was derived from the USGS Landsat Collection 2 Level-2 Science Product (LANDSAT/LC08/C02/T1_L2 and LANDSAT/LC09/C02/T1_L2). All scenes intersecting Dresden between 1 June and 31 August 2023 were included. The Level-2 product provides the ST_B10 band, generated using a single-channel algorithm applied to TIRS Band 10 with atmospheric correction from NCEP/NCAR reanalysis (USGS, 2023).

Clouds, shadows, and cirrus were removed using the QA_PIXEL bitmask (bits 2, 3, and 4). The scaled ST_B10 values were converted to physical temperature using the USGS formula:

$$\text{LST (K)} = \text{ST\_B10} \times 0.00341802 + 149.0$$

$$\text{LST (°C)} = \text{LST (K)} - 273.15$$

A median composite was generated across all cloud-free observations to reduce residual cloud effects and short-term anomalies. The final LST composite was clipped to the Dresden boundary and exported at 30 m resolution in EPSG:32633 (UTM Zone 33N). All maps were visualised in GEE using a graduated colour scale.

4.3 Sentinel-1 SAR Backscatter Processing

Sentinel-1 C-band SAR data were sourced from the COPERNICUS/S1_GRD collection, which provides sigma-nought (σ^0) backscatter in decibels (dB). The GEE catalogue includes

thermal noise removal, radiometric calibration, and Range-Doppler terrain correction using the SRTM DEM.

Only Interferometric Wide (IW) mode scenes from descending orbits with both VV and VH polarisations were used to ensure consistent geometry. Median composites were generated separately for VV and VH. The polarisation ratio was computed as:

$$\text{VV–VH (dB)} = \text{VV (dB)} - \text{VH (dB)}$$

This ratio enhances the contrast between double-bounce dominated urban surfaces (high values) and vegetation-dominated areas (low values). All SAR composites were clipped to the Dresden AOI and exported at 10 m resolution.

4.4 Statistical Analysis and Inter-Sensor Comparison

For inter-sensor comparison, the Sentinel-1 composites were resampled to the 30 m Landsat grid using bilinear interpolation. All four variables (LST, VV, VH, VV–VH) were stacked, and pixels with missing values in any layer were removed to ensure a consistent dataset. The statistical analysis included a pixel-wise scatter plot of VV backscatter versus LST, a Pearson correlation matrix across all variables, box-plot comparisons of built-up and non-built-up areas (using VV > −9 dB as a threshold following Nghiem et al., 2009), a histogram of LST distribution, and a multivariate pair-plot matrix showing all bivariate relationships. Together, these analyses provide a comprehensive characterisation of how thermal and radar properties co-vary across Dresden's urban landscape

5. Results

5.1 Land Surface Temperature Spatial Distribution

Figures 1 and 2 present the summer 2023 LST composite for Dresden as generated and visualised within GEE (rainbow colour scale) and as a georeferenced GeoTIFF product with calibrated temperature legend, respectively. The LST distribution across Dresden ranges from approximately 20°C in densely forested areas and over the Elbe River, to values exceeding 45°C over dark sealed surfaces—primarily flat industrial rooftops, large car park areas, and railway infrastructure—during peak summer conditions.

The spatial organisation of LST clearly reflects the urban morphology of Dresden. The highest temperatures are concentrated in the compact historical city centre south of the Elbe, in western industrial districts, and along major transport corridors and retail zones. The Elbe floodplain constitutes a pronounced thermal cool corridor running east–west through the image, attributable to the combined effects of open water evaporation, riparian vegetation transpiration, and the high thermal inertia of fluvial water bodies. The Dresdner Heide Forest in the northeast appears as the dominant low-LST zone, consistently 8–12°C cooler than adjacent built-up areas at comparable solar exposure. Suburban residential districts interspersed with private gardens exhibit intermediate LST values, reflecting the partial mitigation of surface temperatures by urban vegetation. These patterns are consistent with the established SUHI literature and confirm the physical validity of the LST retrieval.

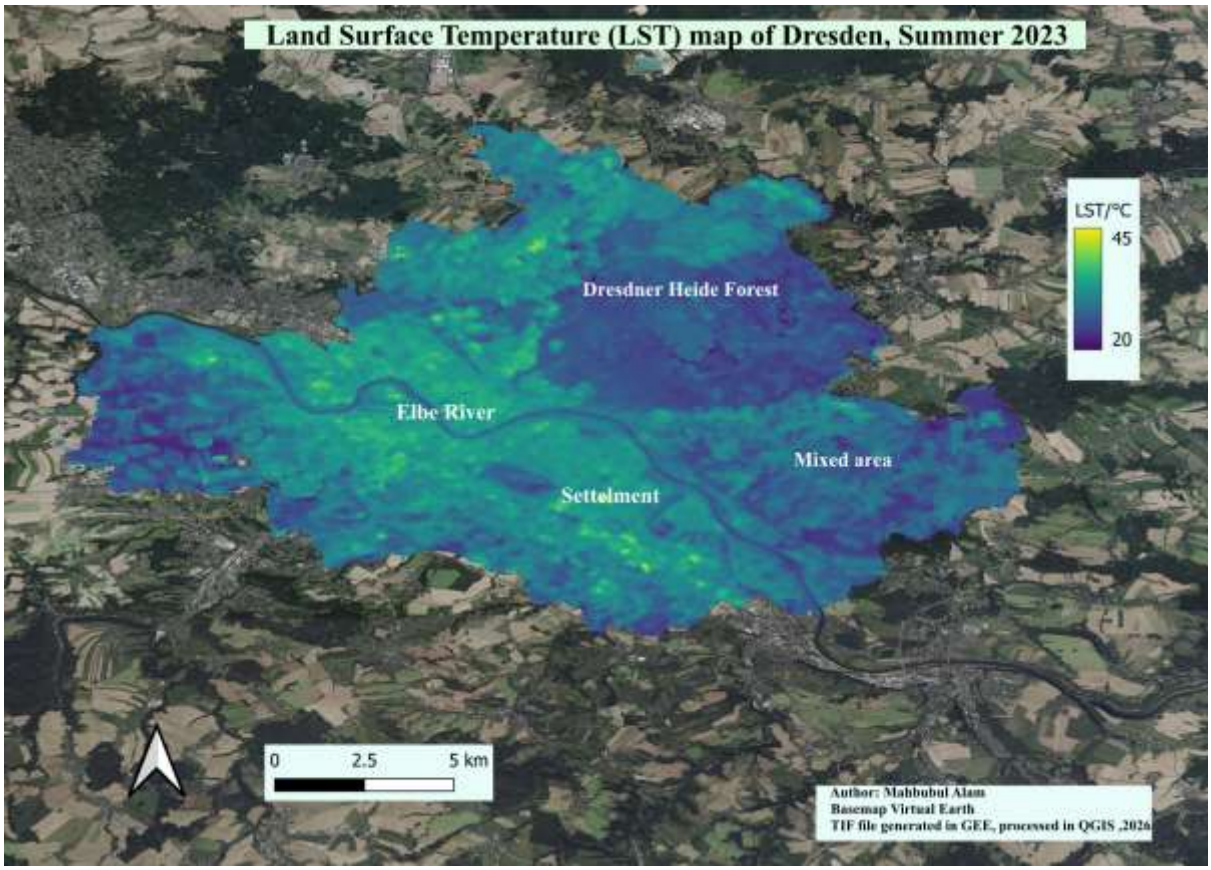

Figure 2. Land Surface Temperature (LST) map of Dresden, summer 2023, as visualised in Google Earth Engine using a rainbow colour palette. Red/warm tones denote high LST (>40°C, sealed urban surfaces); blue/green tones indicate low LST (<25°C, forests and water bodies). Generated in GEE from Landsat 8/9 Collection 2 median composite (June–August 2023).

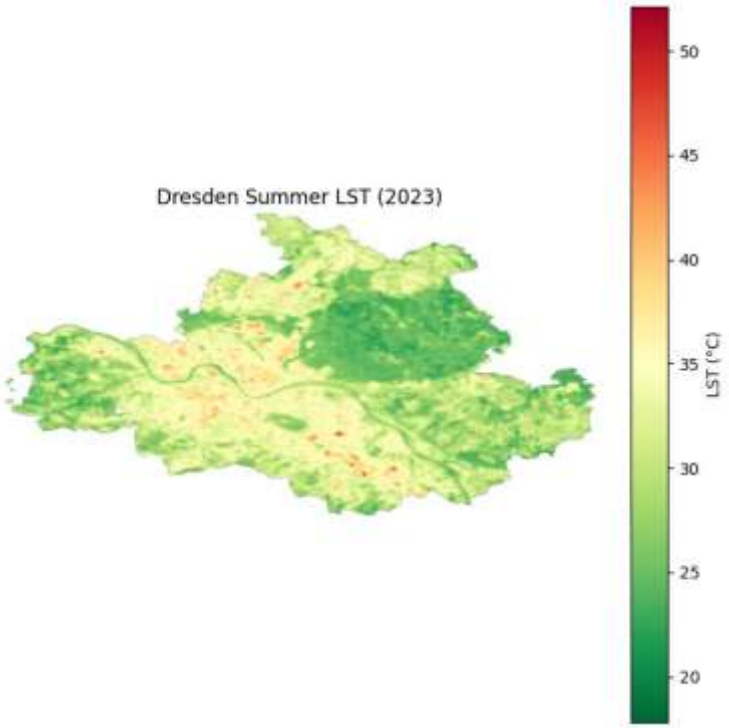

Figure 3. Dresden summer LST (2023) with calibrated physical temperature scale (°C). Hotspots in the city centre and industrial zones, and cool regions in the Dresdner Heide and Elbe floodplain, clearly delineate the surface urban heat island structure.

5.2 Sentinel-1 VV backscatter

The summer 2023 median VV backscatter composite, generated in Google Earth Engine and visualised in QGIS (Figure X), captures the spatial distribution of surface and double-bounce scattering across the Dresden AOI. The colour scale ranges from approximately −25 dB (dark purple) to +19 dB (bright green), with higher values indicating stronger co-polarised radar returns.

Built-up areas in the central and southern parts of Dresden exhibit moderate to high VV backscatter, appearing in bright greenish tones. These elevated values reflect the dominance of surface and double-bounce scattering from building façades, road surfaces, and other engineered structures, which efficiently return C-band energy in VV polarisation. Industrial zones, transport corridors, and compact residential districts are therefore clearly delineated as VV-bright regions.

The Dresdner Heide Forest and other vegetated zones show lower to intermediate VV values, represented by darker green to bluish tones. Vegetation canopies depolarise the incident radar signal through volume scattering, reducing the co-polarised VV return relative to urban surfaces. As a result, forested areas appear systematically darker than the surrounding built-up fabric.

The Elbe River and associated water bodies are mapped as very low VV backscatter (deep purple), consistent with the near-specular reflection of smooth water surfaces that directs most

radar energy away from the sensor. This produces a sharply defined low-VV corridor along the river.

The mixed area in the southeastern part of the AOI displays intermediate VV levels, reflecting its heterogeneous composition of agricultural fields, bare soil patches, scattered settlement, and mixed vegetation. This mosaic of land-cover types produces a blend of surface and volume scattering, yielding VV values between those of dense urban cores and forested or water-dominated regions.

Overall, the VV backscatter pattern aligns with the expected sensitivity of the co-polarised channel to impervious surface density, surface roughness, and urban structural complexity, providing a complementary structural perspective to the LST distribution.

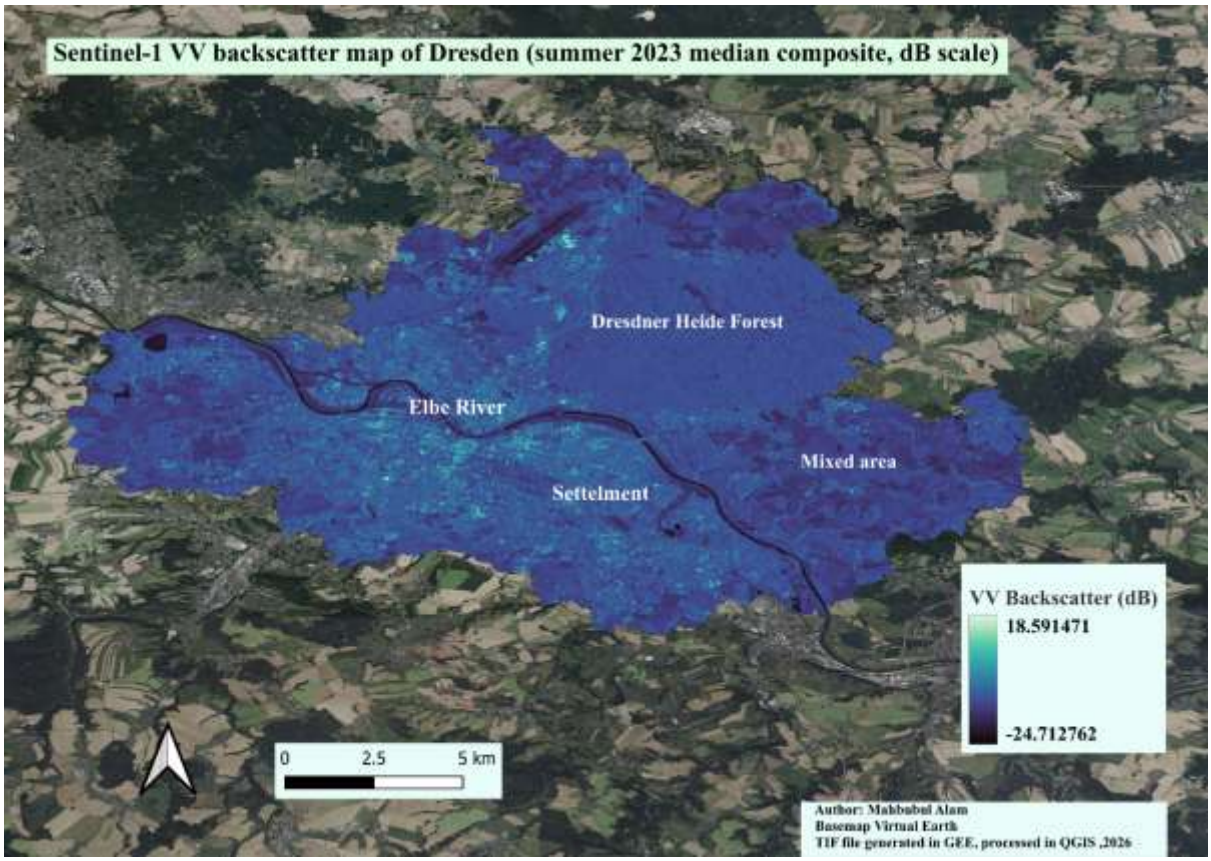

Figure 4. Sentinel-1 VV backscatter map of Dresden (summer 2023 median composite, dB scale), generated in Google Earth Engine and visualised in QGIS. High VV values (bright green) indicate strong surface and double-bounce scattering from urban and other rough surfaces; intermediate values (bluish to green tones) correspond to mixed agricultural, bare soil, and vegetated areas; and low values (dark purple) delineate smooth water bodies and strongly depolarising surfaces such as dense forest

5.3 Sentinel-1 VH Backscatter

The summer 2023 median VH backscatter composite, generated in Google Earth Engine and visualised in QGIS (Figure X), reveals clear spatial contrasts that reflect the depolarised scattering behaviour of different land-cover types. The Plasma colour ramp spans approximately −32 dB (dark purple) to +11 dB (bright yellow), with higher values indicating stronger cross-polarised (VH) returns.

Built-up areas across Dresden exhibit the highest VH backscatter, appearing in bright yellow tones. This is characteristic of urban environments, where radar energy interacts with numerous angular surfaces, façade edges, roof structures, and small vegetation patches. These complex geometries generate strong diffuse and depolarised returns, resulting in elevated VH values.

The Dresdner Heide Forest and other vegetated zones display intermediate VH levels, represented by orange to pinkish-purple tones. These moderate values reflect volume scattering within canopy structures, where radar energy undergoes multiple interactions with leaves and branches. This produces a depolarised signal, but not as strong as the multi-angle scattering typical of dense urban fabric.

The Elbe River and its tributaries appear as very low backscatter regions (deep purple). Smooth water surfaces act as specular reflectors, directing most radar energy away from the sensor and producing minimal depolarised return. This creates a sharp contrast between the river network and the surrounding land cover.

A small low-backscatter patch in the northeastern part of the study area forms a uniform dark-purple zone. Its consistently low reflectivity suggests a surface with minimal structural roughness or moisture-related scattering, although its exact land-cover type cannot be determined from VH backscatter alone and requires further verification.

Overall, the VH backscatter distribution highlights the sensitivity of the cross-polarised channel to structural complexity, canopy volume, and diffuse scattering, complementing the VV-based interpretation of urban and vegetated surfaces.

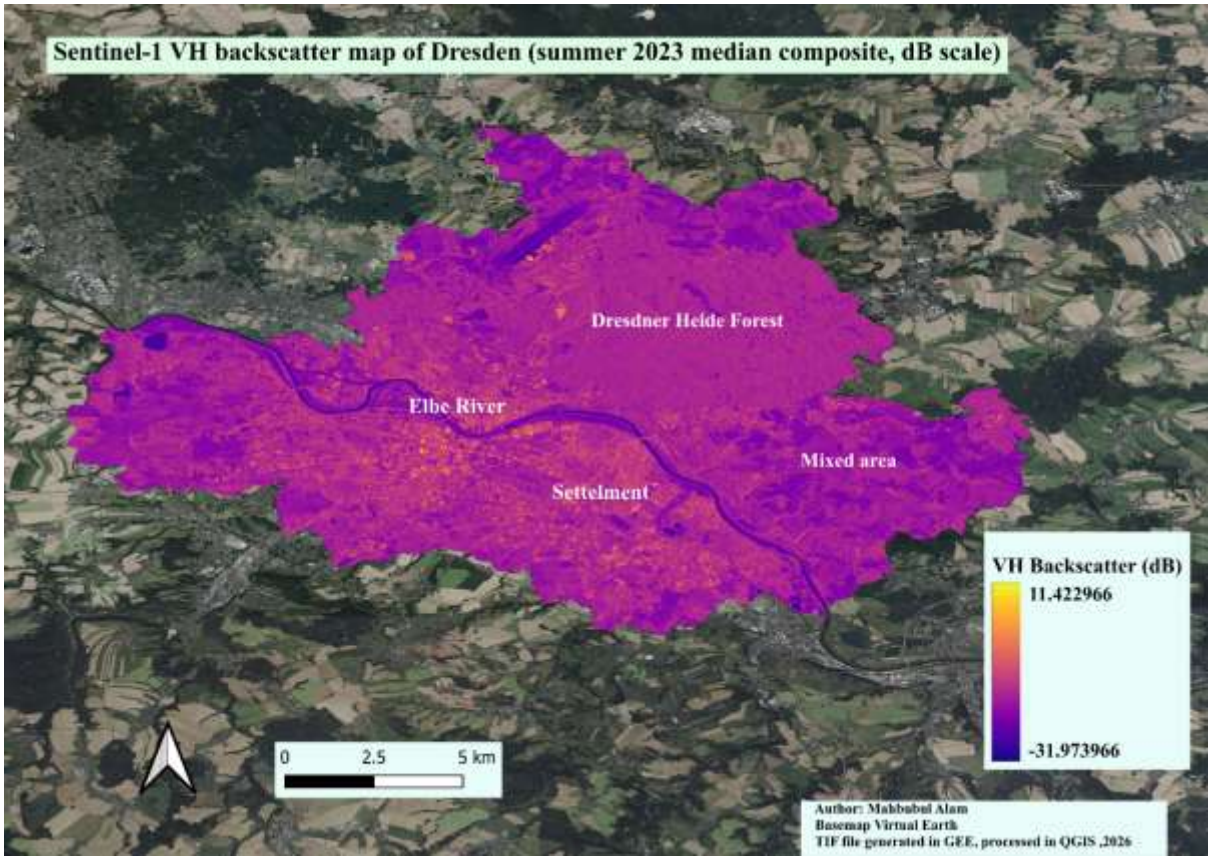

*Figure 5. Sentinel-1 VH backscatter map of Dresden (summer 2023 median composite, dB scale), generated in Google Earth Engine and visualised in QGIS using the Plasma colour ramp. High VH values (bright yellow) indicate strong depolarised returns from complex urban structures; intermediate values (orange to pink-purple) correspond to vegetation-dominated areas with volume scattering; and low values (dark purple) delineate smooth water bodies and other surfaces with minimal depolarised backscatte*r.

5.4 VV–VH Polarisation Ratio

The VV–VH polarisation ratio composite (Figure 4), calculated in Google Earth Engine as the arithmetic difference between the median VV and VH backscatter images (in dB), provides a structurally sensitive indicator of scattering behaviour across Dresden. The colour scale used in the map ("Dresden_VVVH_ratio_2023_summer") ranges from approximately –9 dB to +31 dB, with warm yellow-green tones representing high ratio values and purple-blue tones indicating low ratios.

Urban areas exhibit the highest VV–VH ratios, appearing in bright yellow-green. These elevated values reflect the dominance of surface and double-bounce scattering from buildings, road networks, and engineered structures, where VV backscatter is substantially stronger than VH. As a result, the compact city centre, dense residential districts, and major transport corridors are clearly delineated as high-ratio zones**.**

The Dresdner Heide Forest and other vegetated regions display intermediate ratio values, shown in green-blue tones. Vegetation produces stronger VH relative to VV due to volume

scattering within canopy layers, resulting in lower ratios than those found in urban areas but higher than those over water.

The mixed area in the southeastern part of the study region represents a heterogeneous peri-urban landscape composed of scattered settlement, mixed vegetation, bare soil, and agricultural land. This mosaic of land-cover types produces a combination of surface, volume, and soil scattering, resulting in intermediate VV–VH ratios. The spatial variability in this zone reflects the transition between urban periphery and rural land uses rather than a topographic effect.

The Elbe River and other smooth water bodies appear as very low-ratio regions (deep purple). Both VV and VH backscatter are strongly suppressed over water, and because the two channels are similarly weak, the ratio remains low and less structurally meaningful for this surface type.

Overall, the spatial distribution of the VV–VH ratio corresponds closely with known patterns of urban density, vegetation cover, and peri-urban land-use mosaics across Dresden. This confirms the utility of the VV–VH ratio as a robust proxy for impervious surface intensity, structural complexity, and land-cover heterogeneity.

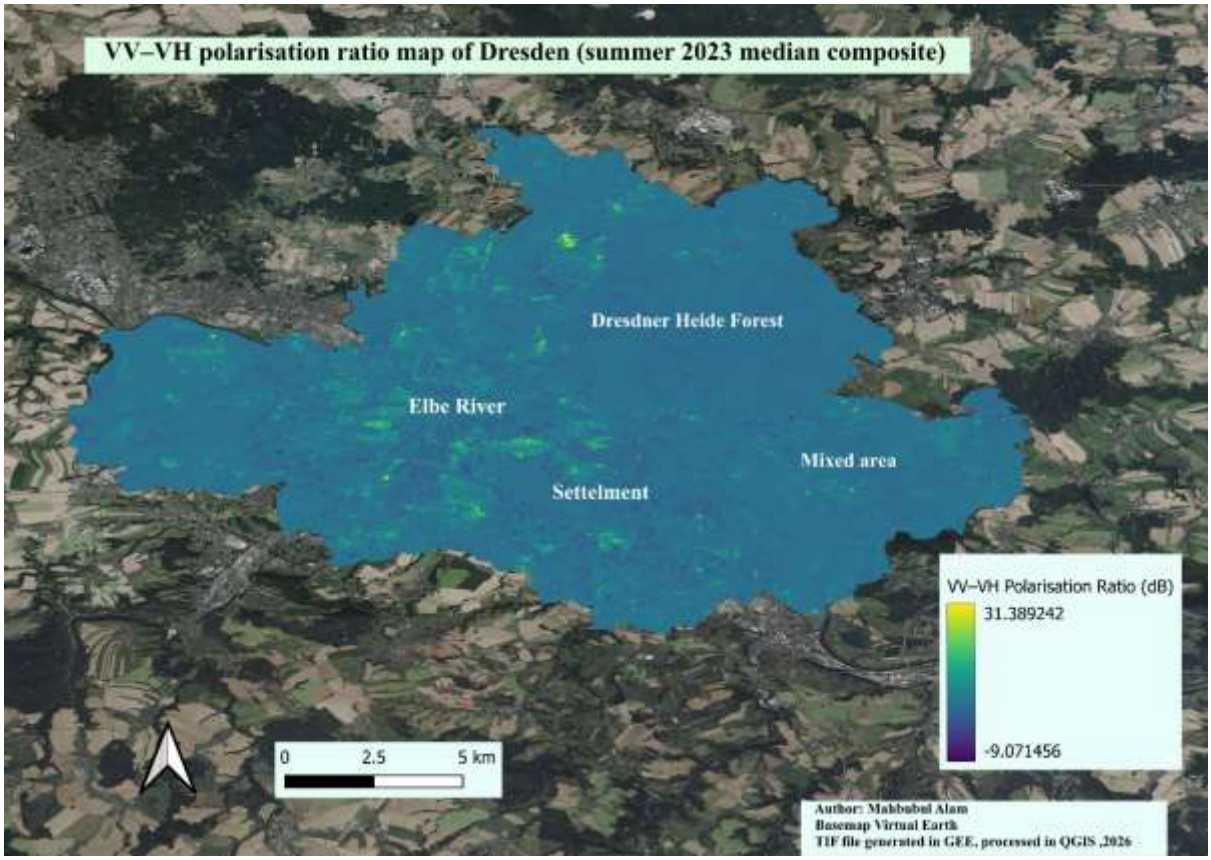

Figure 6. *VV–VH polarisation ratio map of Dresden (summer 2023 median composite), generated in Google Earth Engine and visualised in QGIS. High ratio values (yellow-green) indicate strong VV dominance associated with surface and double-bounce scattering from urban structures. Intermediate values (green-blue) represent vegetation and heterogeneous peri-urban land cover, while low values (purple) correspond to smooth surfaces such as water.*

5.5 Interpretation of Backscatter–LST Relationships and Range Differences Between Maps and Scatter Plots

5.4..1Visualisation Ranges vs. Raw Data Ranges

The backscatter ranges displayed in the maps (VV ≈ −25 to +18 dB; VH ≈ −32 to +11 dB; VV–VH ≈ −9 to +31 dB) represent **visualisation ranges** produced by QGIS. During map rendering, QGIS applies several contrast-enhancement operations, including:

- **min–max stretching**,
- **histogram compression**,
- **colour-ramp normalisation**, and
- **clipping of extreme values**.

These operations do not alter the underlying pixel values; instead, they optimise the visual contrast so that spatial patterns are more interpretable. Consequently, the displayed range is often narrower or slightly shifted relative to the true physical values.

In contrast, the scatter plot uses the **raw, unmodified backscatter values** exported directly from Google Earth Engine or QGIS. These values typically span a slightly wider or differently centred range (e.g., VV ≈ −22 to +22 dB), because no stretching or clipping is applied. The scatter plot therefore reflects the **true radiometric distribution** of the dataset.

The mismatch between map ranges and scatter-plot ranges is therefore **normal, expected, and scientifically valid**. It does not indicate any inconsistency in the data; rather, it reflects the difference between:

1. **visualisation ranges** (optimised for cartographic clarity), and
2. **statistical ranges** (representing the actual physical measurements).

5.4.2 Pixel-Wise LST vs. VV Backscatter Scatter Analysis

Figure 5 presents the pixel-wise scatter plot between VV backscatter and LST across all valid pixels within the Dresden AOI. The distribution spans a VV range of approximately −22 to +22 dB and an LST range of roughly 20°C to 52°C. The scatter cloud exhibits a diffuse but recognisable positive trend: pixels with moderate to high VV backscatter (approximately −10 to +10 dB), typically associated with built-up surfaces, show a broad LST distribution skewed toward higher temperatures (30–45°C). In contrast, pixels with very low VV backscatter (< −15 dB), corresponding to vegetation, water, and smooth agricultural surfaces, cluster predominantly within the cooler LST range (20–30°C).

The wide scatter reflects the combined influence of mixed pixels, surface moisture variability, building material differences, and the directional sensitivity of SAR to building orientation—factors that do not directly influence LST. A dense core of observations in the VV range −15 to −5 dB and LST range 25–38°C represents the dominant suburban residential fabric of Dresden, where moderate structural complexity and moderate thermal loading coexist.

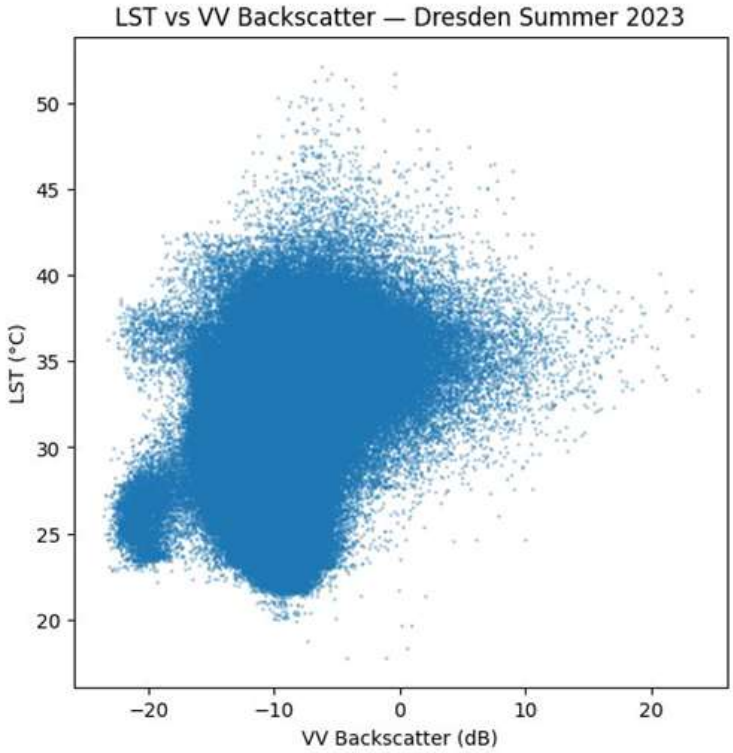

Figure 7. *Figure 7: Pixel-wise scatter plot of Sentinel-1 VV backscatter (dB) versus Landsat-derived LST (°C) for Dresden, summer 2023. The weak positive association between VV backscatter and LST reflects the co-spatial relationship between built-up density and surface urban heat island intensity. Differences between map ranges and scatter-plot ranges arise from QGIS visualisation stretching and do not indicate any inconsistency in the underlying data.*

5.5 Pearson Correlation Matrix

Figure 6 shows the Pearson correlation heatmap among LST, VV, VH, and VV–VH variables. The most noteworthy findings are as follows. LST exhibits a positive but moderate correlation with VV (r = 0.28) and a weaker positive correlation with both VH (r = 0.18) and the VV–VH ratio (r = 0.19). These values are consistent with those reported in comparable urban studies (Zhang et al., 2016) and reflect the inherent confounding factors discussed above. The strong correlation between VV and VH (r = 0.81) is expected, as both polarisations respond to the general intensity of microwave scattering across all mechanisms present in a given pixel, and thus track the broad land cover gradient (urban vs. vegetated vs. water) in a consistent manner. The negative correlation between VH and the VV–VH ratio (r = −0.24) is also physically expected: high VH values—associated with vegetation—inherently suppress the VV–VH difference, while low VH values—associated with smooth or double-bounce dominated surfaces—tend to yield a larger VV–VH contrast.

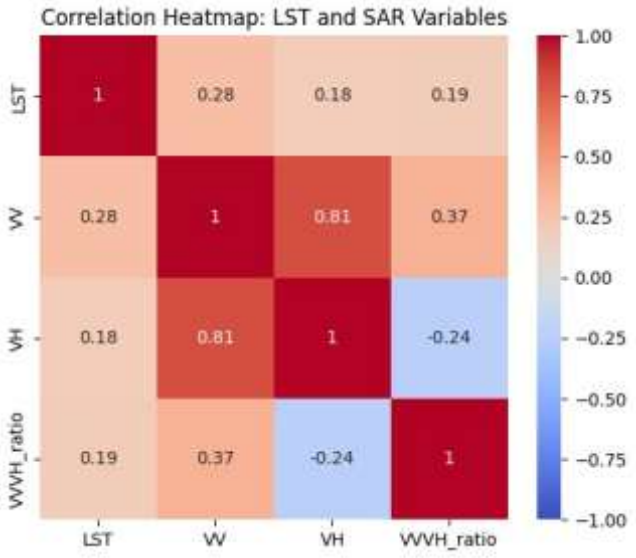

Figure 8. Pearson correlation heatmap among LST (°C), VV (dB), VH (dB), and VV–VH ratio (dB) for all valid co-located pixels within the Dresden AOI, summer 2023. Positive correlations are shown in red; negative correlations in blue.

5.6 Land Cover Stratified LST and VV Comparison

Figures 7 and 8 present box plots of LST and VV backscatter, respectively, stratified between built-up pixels (classified as VV > −9 dB) and all other pixels. Several noteworthy observations emerge from these comparisons. The LST box plot (Figure 7) reveals that the median LST in the built-up category (approximately 30°C) is paradoxically lower than in the 'Other' category (approximately 34°C), with the built-up class displaying a considerably wider interquartile range. This counterintuitive result warrants interpretation: the VV > −9 dB threshold captures not only dense urban cores—which indeed exhibit high LST—but also a heterogeneous mix of urban land cover types including partially vegetated residential areas, industrial buildings with varying thermal properties, and wet surfaces encountered during overpass times. The 'Other' category includes open fields, bare agricultural soils, and large-format impervious surfaces that may lack significant double-bounce but generate elevated LST. Moreover, the summer median compositing integrates observations across varying solar angles and atmospheric conditions, potentially introducing systematic differences between VV classes.

The VV box plot (Figure 8) confirms the expected pattern: built-up pixels exhibit higher VV backscatter on average (median approximately −9 dB) compared to the non-built-up category (median approximately −7 dB), with both classes showing wide distributions and numerous outliers attributable to the heterogeneous land cover types captured within each class. The overlap of VV distributions between classes is consistent with the moderate rather than strong LST-SAR correlations reported in the correlation matrix.

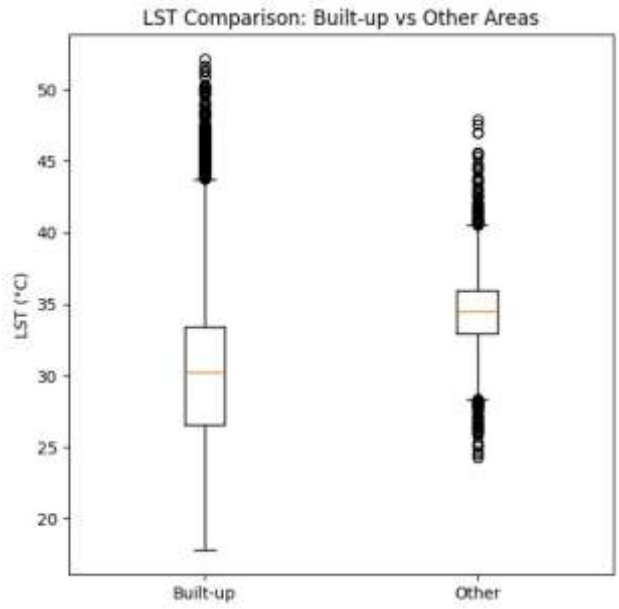

Figure 9. Box plot of LST (°C) stratified by land cover category (built-up: VV > −9 dB; Other: remaining pixels) for Dresden, summer 2023. Medians, interquartile ranges, whiskers, and outliers are shown.

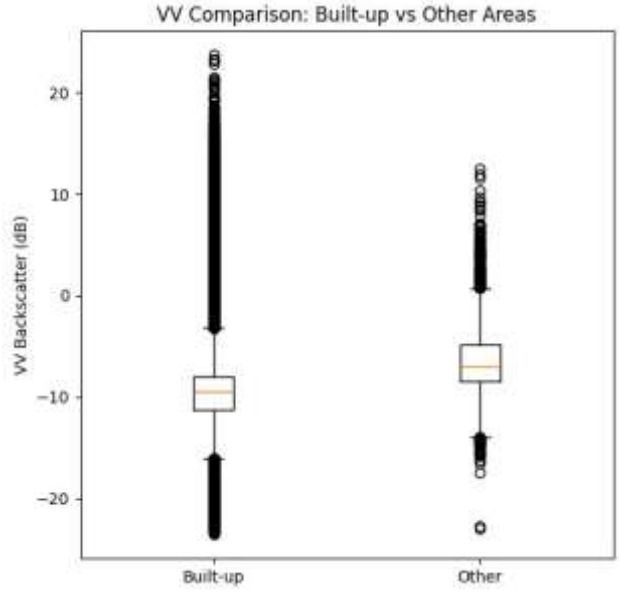

Figure 10. Box plot of Sentinel-1 VV backscatter (dB) stratified by built-up versus other land cover categories, Dresden summer 2023.

5.7 LST Frequency Distribution

The histogram of LST values across the entire Dresden administrative area (Figure 9) reveals a broad distribution spanning approximately 20–44°C, with a characteristic bimodal structure. The primary mode occurs at approximately 24–26°C, corresponding to the cool Dresdner Heide forest and Elbe floodplain areas that constitute a substantial fraction of the administrative area. A secondary, broader mode spanning approximately 28–36°C reflects the large fraction of suburban residential and mixed urban land cover that dominates the built-up portion of Dresden. The tail above approximately 38°C represents the small but thermally extreme

hotspots associated with highly sealed, low-albedo industrial and commercial surfaces. The bimodal structure is thus physically meaningful and consistent with the land cover composition of Dresden, providing validation of the LST retrieval quality.

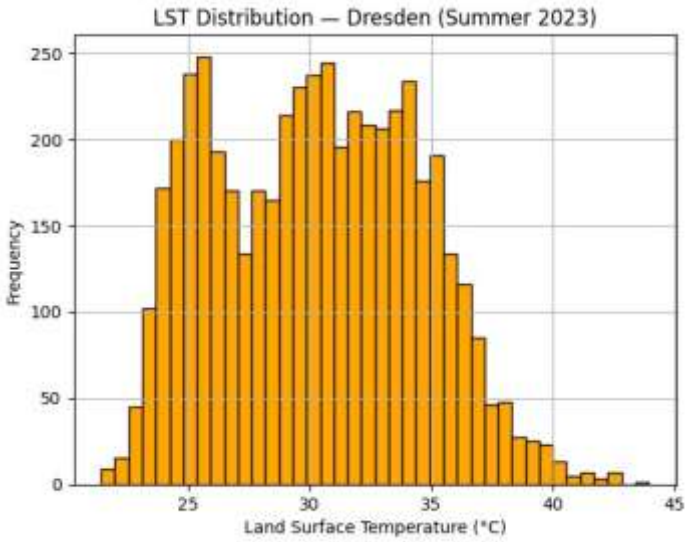

Figure 11. Frequency histogram of LST values (°C) across the Dresden administrative area, summer 2023. The bimodal distribution reflects the thermal contrast between forested/vegetated areas (~24–26°C) and built-up/sealed surfaces (~28–36°C).

5.9 Multivariate Pair Plot

The pair plot matrix in Figure 10 provides a comprehensive visualisation of all bivariate relationships among LST, VV, VH, and VV–VH variables. The diagonal histograms confirm the distributional characteristics of each variable individually: LST exhibits the bimodal distribution described above; VV shows a strongly right-skewed distribution with a sharp mode near −10 to −12 dB (consistent with the prevalence of vegetated and mixed suburban surfaces); VH is similarly right-skewed with its mode near −15 dB; and the VV–VH ratio is highly leptokurtic, concentrated near 4–6 dB with a long right tail from urban double-bounce hotspots. The off-diagonal scatter plots confirm the diffuse positive LST-VV and LST-VH associations, the strong VV-VH linear relationship, and the negative VH–VV/VH ratio relationship discussed in Section 5.5. The overall pattern is internally consistent and physically interpretable.

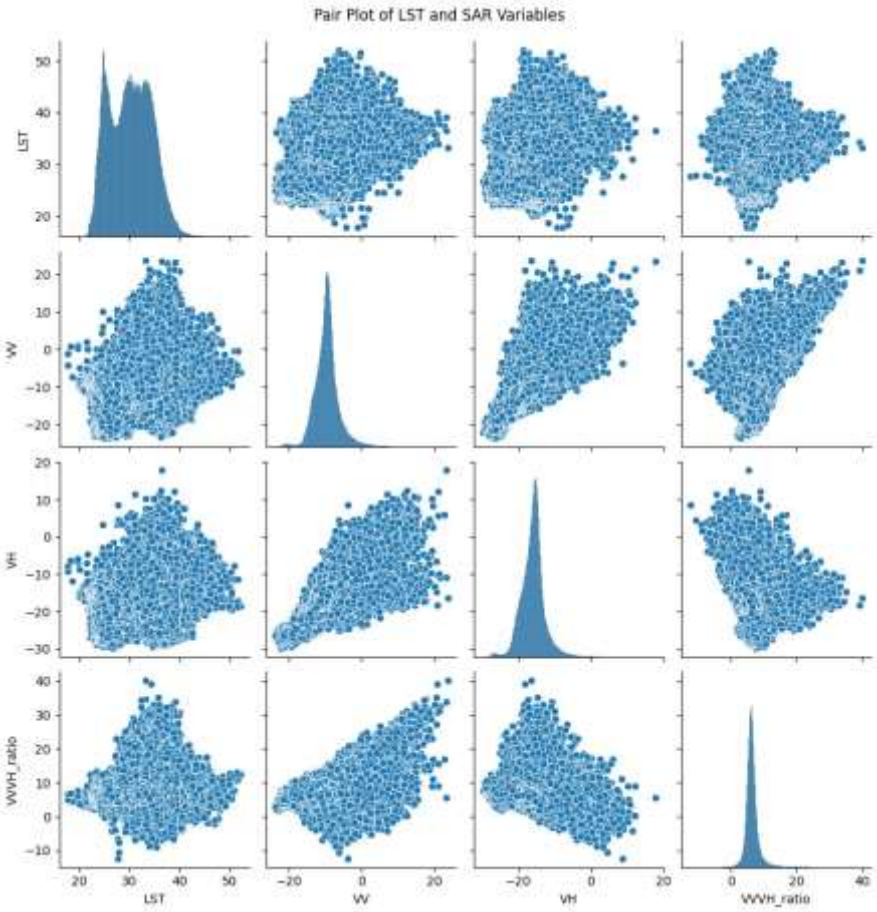

Figure 12. Pair plot matrix of LST (°C), VV (dB), VH (dB), and VV–VH ratio (dB) for all valid co-located pixels within the Dresden AOI, summer 2023. Diagonal panels show univariate histograms; off-diagonal panels show bivariate scatter plots.

6. Discussion

6.1 Physical Interpretation of LST–SAR Spatial Correspondence

The spatial and statistical analyses collectively demonstrate that the thermal and structural properties of Dresden's urban landscape are closely linked, consistent with established theory on urban surface processes. The positive association between LST and VV backscatter reflects their shared dependence on impervious surface density and built-up morphology. Surfaces that generate strong VV returns—primarily building façades, sealed pavements, and engineered materials—also exhibit high thermal inertia, reduced evapotranspiration, and lower albedo, all of which contribute to elevated daytime LST (Oke, 1982; Voogt & Oke, 2003). Conversely, vegetated areas, which produce enhanced VH through volumetric scattering and lower VV–VH ratios, maintain cooler surface temperatures due to canopy shading and latent heat fluxes (Yuan & Bauer, 2007).

The VV–VH ratio provides an additional structural indicator that aligns well with thermal patterns. Although its correlation with LST ($r = 0.19$) is weaker than that of VV alone, the ratio is more directly tied to urban structural density because it suppresses common-mode variations affecting both VV and VH. The spatial coincidence between high VV–VH ratio zones—dense residential districts, industrial complexes, and the compact city centre—and the LST hotspots

observed in Figures 1–2 and 4 reinforces the interpretation that thermal and radar-derived structural metrics respond to similar underlying land-cover gradients. The diffuse nature of the pixel-wise correlations is therefore not a contradiction but a reflection of the heterogeneous and mixed-pixel character of Dresden's urban fabric.

6.2 Critical Analysis: Explaining the Counterintuitive Box-Plot Result

The finding that pixels classified as "built-up" using a simple VV > −9 dB threshold exhibit a lower median LST than the remaining pixels is counterintuitive and appears inconsistent with both the SUHI literature and the positive VV–LST relationship established earlier. However, this discrepancy arises from three interacting classification artefacts that highlight the limitations of threshold-based SAR stratification in heterogeneous urban environments.

First, the VV > −9 dB threshold is inherently impure. While it successfully captures many dense urban surfaces, it also includes suburban residential areas with substantial vegetation, peri-urban structures, and agricultural facilities. These surfaces may produce elevated VV due to corner reflectors (e.g., fences, isolated buildings, machinery) but maintain lower LST because of surrounding vegetation or shading.

Second, the "non-built-up" class (VV ≤ −9 dB) is not thermally homogeneous. It includes both cool forested areas and thermally extreme bare agricultural soils, which can exceed 38°C under summer conditions due to low moisture retention and minimal shading. These hot agricultural pixels inflate the median LST of the "non-built-up" class, producing an apparent inversion of expected SUHI patterns.

Third, the −9 dB threshold originates from global-scale urban mapping studies (Nghiem et al., 2009) and is optimised for large, dense megacities rather than the morphologically diverse structure of a medium-sized Central European city. Industrial rooftops, for example, often produce specular reflections that suppress VV below −9 dB despite being among the hottest surfaces in Dresden.

Together, these factors demonstrate that single-threshold SAR classification is insufficient for thermally meaningful land-cover stratification. The results strongly support the adoption of multivariate supervised approaches—incorporating spectral indices, DSM-derived height metrics, and SAR texture features—to more accurately distinguish thermally relevant surface types in future work.

6.3 Methodological Strengths

Despite the limitations identified above, the study benefits from several methodological strengths that enhance the robustness and reproducibility of the results.

First, the use of Google Earth Engine ensures full transparency and repeatability: the entire workflow—from data ingestion to compositing and export—can be re-executed with minimal user intervention, leveraging continuously updated satellite archives. Second, the use of seasonal median compositing across a full three-month summer period reduces the influence of transient anomalies such as cloud shadows, rainfall-induced soil moisture spikes, or short-term heat-wave variability. This produces a more stable representation of the underlying thermal and structural state of the urban surface than would be possible from single-date imagery.

Third, the multi-metric statistical framework—combining scatter plots, correlation matrices, box-plot comparisons, histograms, and a multivariate pair plot—provides a comprehensive characterisation of the LST–SAR relationship. This integrated approach reveals not only the expected positive associations between structural complexity and surface temperature but also the methodological tensions introduced by mixed pixels, land-cover heterogeneity, and threshold-based classification. The consistency of patterns across independent metrics strengthens confidence in the physical validity of the findings

7. Limitations

This study is subject to several methodological limitations that influence the interpretation and generalisability of its findings. The most fundamental constraint arises from the spatial resolution mismatch between Landsat-derived LST and Sentinel-1 SAR backscatter. Although both datasets were harmonised to a 30 m grid, the effective thermal footprint of the Landsat TIRS sensor is considerably larger than its nominal resolution, while the native 10 m SAR signal captures structural variability at much finer scales. As a result, many pixels—particularly in Dresden's heterogeneous suburban areas—represent mixtures of impervious, vegetated, and bare surfaces, introducing unavoidable mixed-pixel effects that contribute to the diffuse character of the LST–SAR relationships.

A second limitation concerns the use of a single VV backscatter threshold to distinguish built-up from non-built-up areas. While widely applied in global urban mapping, this threshold does not adequately reflect the morphological diversity of Dresden. It misclassifies cool suburban pixels with high VV caused by corner reflectors, and simultaneously excludes thermally extreme industrial rooftops that produce low VV due to specular reflection. This classification impurity explains the counterintuitive box-plot result and highlights the need for multivariate or supervised approaches that incorporate additional SAR and optical indicators.

Temporal representativeness also poses a constraint. The median composites used in this study provide a stable seasonal characterisation but inevitably blend observations from different dates and atmospheric conditions. For LST, variations in cloud cover and overpass timing introduce subtle temporal biases, while SAR backscatter remains sensitive to episodic moisture events that are only partially suppressed by the median. Consequently, the composites represent an aggregated summer state rather than strictly synchronous thermal and structural conditions.

Further limitations arise from the geometric properties of SAR imaging. Layover, shadow, and azimuth-dependent double-bounce effects introduce structural artefacts that have no equivalent in nadir-viewing thermal imagery. These distortions systematically alter VV and VV–VH values near tall buildings and along streets aligned with the radar look direction, adding noise to the LST–SAR scatter relationships that cannot be fully corrected without multi-orbit data.

The absence of in situ validation represents an additional constraint. Neither the LST nor SAR products were compared against ground-based measurements, meaning that the absolute accuracy of the retrieved values relies on published algorithm validations rather than local calibration. While the spatial patterns remain robust, the lack of field data limits the assessment of absolute temperature and backscatter accuracy for Dresden.

Finally, the analysis is restricted to a single summer season (2023), which was anomalously warm. Although this provides insight into extreme SUHI conditions, it limits the

generalisability of the quantitative relationships observed. Interannual variability in vegetation moisture, soil conditions, and heat-wave frequency may substantially influence LST–SAR coupling. Multi-year analyses would be required to establish climatologically representative patterns and to assess the stability of the observed relationships over time.

8. Conclusion

This study demonstrates the value of integrating thermal infrared observations from Landsat 8/9 with C-band SAR backscatter from Sentinel-1 to analyse the structural and thermal characteristics of Dresden during the summer of 2023. By combining LST, VV, VH, and the VV–VH polarisation ratio within a unified Google Earth Engine workflow, the analysis provides a multi-sensor perspective on how urban morphology, vegetation cover, and surface materials jointly shape the spatial pattern of surface temperatures across a heterogeneous Central European city.

The results show a consistent, physically interpretable relationship between thermal and radar-derived structural metrics. Built-up areas characterised by strong VV backscatter and high VV–VH ratios correspond to elevated LST, reflecting the combined influence of impervious materials, reduced evapotranspiration, and enhanced double-bounce scattering. Vegetated areas, in contrast, exhibit low VV, higher VH, and lower VV–VH ratios, and maintain substantially cooler surface temperatures. Although the pixel-wise correlations between LST and SAR variables are moderate, their spatial correspondence is clear and robust, confirming that thermal and structural indicators respond to the same underlying land-cover gradients.

The study also highlights important methodological insights. The counterintuitive box-plot result—where the VV-defined "built-up" class exhibited lower median LST than the "non-built-up" class—demonstrates the limitations of single-threshold SAR classification in morphologically diverse urban environments. This finding underscores the need for multivariate or supervised classification approaches that incorporate both SAR and optical information to achieve thermally meaningful land-cover stratification. Furthermore, the analysis reveals how mixed-pixel effects, SAR geometric distortions, and temporal compositing influence the strength and clarity of LST–SAR relationships.

Despite these limitations, the study successfully illustrates the complementary strengths of thermal and SAR data for urban surface characterisation. The workflow developed here is fully reproducible, scalable, and adaptable to other cities, and it demonstrates the potential of cloud-based platforms such as GEE for rapid, transparent, and large-scale environmental analysis. The findings provide a foundation for more advanced future work, including multi-year SUHI assessments, supervised land-cover classification, SAR texture analysis, and the integration of higher-resolution thermal datasets.

Overall, this research contributes to a growing body of evidence that multi-sensor approaches offer a more complete understanding of urban surface processes than any single data source alone. By linking structural complexity with thermal behaviour, the study provides insights that are relevant for urban climate analysis, heat-mitigation planning, and the broader field of urban remote sensing.

11. References

1. Antropov, O., Rauste, Y., Väänänen, A., Mutanen, T., & Häme, T. (2014). Land cover and soil type mapping from spaceborne PolSAR data at L-band with probabilistic neural network. *IEEE Transactions on Geoscience and Remote Sensing*, *52*(9), 5256–5270.

2. Barsi, J. A., Lee, K., Kvaran, G., Markham, B. L., & Pedelty, J. A. (2014). The spectral response of the Landsat-8 operational land imager. *Remote Sensing*, *6*(10), 10232–10251.

3. Brunner, D., Lemoine, G., & Bruzzone, L. (2010). Earthquake damage assessment of buildings using VHR optical and SAR imagery. *IEEE Transactions on Geoscience and Remote Sensing*, *48*(5), 2403–2420.

4. City of Dresden. (2023). *Stadtgrün und Wald*. Landeshauptstadt Dresden.

5. Cloude, S. R., & Pottier, E. (1996). A review of target decomposition theorems in radar polarimetry. *IEEE Transactions on Geoscience and Remote Sensing*, *34*(2), 498–518.

6. Deutscher Wetterdienst (DWD). (2023). *Klimadaten Deutschland*. https://www.dwd.de

7. Dong, J., Metternicht, G., Hostert, P., Fensholt, R., & Chowdhury, R. R. (2019). Remote sensing and geospatial technologies in support of a normative land system science. *Current Opinion in Environmental Sustainability*, *38*, 9–17.

8. Esch, T., Marconcini, M., Felbier, A., Roth, A., Heldens, W., Huber, M., Schwinger, M., Taubenböck, H., Müller, A., & Dech, S. (2013). Urban footprint processor — Fully automated processing chain generating settlement masks from global data of the TanDEM-X mission. *IEEE Geoscience and Remote Sensing Letters*, *10*(6), 1617–1621.

9. Gabriel, K. M. A., & Endlicher, W. R. (2011). Urban and rural mortality rates during heat waves in Berlin and Brandenburg, Germany. *Environmental Pollution*, *159*(8–9), 2044–2050.

10. Gorelick, N., Hancher, M., Dixon, M., Ilyushchenko, S., Thau, D., & Moore, R. (2017). Google Earth Engine: Planetary-scale geospatial analysis for everyone. *Remote Sensing of Environment*, *202*, 18–27.

11. Howard, L. (1833). *The climate of London* (Vol. 1). Harvey and Darton.

12. Li, Z.-L., Tang, B.-H., Wu, H., Ren, H., Yan, G., Wan, Z., Trigo, I. F., & Sobrino, J. A. (2013). Satellite-derived land surface temperature: Current status and perspectives. *Remote Sensing of Environment*, *131*, 14–37.

13. Nghiem, S. V., Balk, D., Rodriguez, E., Neumann, G., Sorichetta, A., Small, C., & Elvidge, C. D. (2009). Observations of urban and suburban environments with global

satellite scatterometer data. *ISPRS Journal of Photogrammetry and Remote Sensing*, *64*(4), 367–380.

14. Oke, T. R. (1982). The energetic basis of the urban heat island. *Quarterly Journal of the Royal Meteorological Society*, *108*(455), 1–24.
15. OpenStreetMap Contributors. (2023). *OpenStreetMap* [Geographic data]. https://www.openstreetmap.org
16. Statistical Office of Saxony. (2023). *Statistisches Jahrbuch Sachsen*. Statistisches Landesamt des Freistaates Sachsen.
17. Stathopoulou, M., & Cartalis, C. (2007). Daytime urban heat islands from Landsat ETM+ and Corine land cover data: An application to major cities in Greece. *Solar Energy*, *81*(3), 358–368.
18. Torres, R., Snoeij, P., Geudtner, D., Bibby, D., Davidson, M., Attema, E., Potin, P., Rommen, B., Floury, N., Brown, M., Traver, I. N., Deghaye, P., Duesmann, B., Rosich, B., Miranda, N., Bruno, C., L'Abbate, M., Croci, R., Pietropaolo, A., & Rostan, F. (2012). GMES Sentinel-1 mission. *Remote Sensing of Environment*, *120*, 9–24.
19. Ulaby, F. T., Moore, R. K., & Fung, A. K. (1982). *Microwave remote sensing: Active and passive* (Vol. 2). Addison-Wesley.
20. USGS. (2023). *Landsat Collection 2 Level-2 science product guide*. U.S. Geological Survey. https://www.usgs.gov/landsat-missions
21. Voogt, J. A., & Oke, T. R. (2003). Thermal remote sensing of urban climates. *Remote Sensing of Environment*, *86*(3), 370–384.
22. Weng, Q. (2009). Thermal infrared remote sensing for urban climate and environmental studies: Methods, applications, and trends. *ISPRS Journal of Photogrammetry and Remote Sensing*, *64*(4), 335–344.
23. Yuan, F., & Bauer, M. E. (2007). Comparison of impervious surface area and normalized difference vegetation index as indicators of surface urban heat island effects in Landsat imagery. *Remote Sensing of Environment*, *106*(3), 375–386.
24. Zhang, Y., Odeh, I., & Han, C. (2016). Bi-temporal characterization of land surface temperature in relation to impervious surface area, NDVI and NDBI, using a sub-pixel image analysis. *International Journal of Applied Earth Observation and Geoinformation*, *13*(6), 827–835.
25. Zhou, D., Zhao, S., Zhang, L., Sun, G., & Liu, Y. (2014). The footprint of urban heat island effect in China. *Scientific Reports*, *4*, 5531.
26. Mund, J.-P. (2025). *Advanced Remote Sensing Innovations (ARSI): Thermal Remote Sensing & SAR Fundamentals* [Lecture slides]. Hochschule für nachhaltige Entwicklung Eberswalde (HNEE).